Journal of Marine Science and Technology

Volume 23 | Issue 2 Article 7

A LINEARLY CONSTRAINED SIGNAL SUBSPACE PROJECTION APPROACH DEVELOPED TO DETECT TARGETS IN HYPERSPECTRAL IMAGES

Zay-Shing Tang
Department of Electrical Engineering, National Taiwan Ocean University, Keelung, Taiwan, R.O.C.

Lena Chang
Department of Communications, Navigation and Control Engineering, National Taiwan Ocean University, Keelung, Taiwan, R.O.C., lenachang@mail.ntou.edu.tw

Hsien-Sen Hung
Department of Electrical Engineering, National Taiwan Ocean University, Keelung, Taiwan, R.O.C.

Recommended Citation

Tang, Zay-Shing; Chang, Lena; and Hung, Hsien-Sen (2015) "A LINEARLY CONSTRAINED SIGNAL SUBSPACE PROJECTION APPROACH DEVELOPED TO DETECT TARGETS IN HYPERSPECTRAL IMAGES," *Journal of Marine Science and Technology*: Vol. 23: Iss. 2, Article 7.
DOI: 10.6119/JMST-014-0430-2
Available at: https://jmstt.ntou.edu.tw/journal/vol23/iss2/7

Journal of Marine Science and Technology, Vol. 23, No. 2, pp. 191-201 (2015)
DOI: 10.6119/JMST-014-0430-2

A LINEARLY CONSTRAINED SIGNAL SUBSPACE PROJECTION APPROACH DEVELOPED TO DETECT TARGETS IN HYPERSPECTRAL IMAGES

Zay-Shing Tang[1], Lena Chang[2], and Hsien-Sen Hung[1]

Key words: hyperspectral image, target detection, optimal filter, multiple constraints, signal subspace projection (SSP), K-means.

ABSTRACT

Hyperspectral images have been widely used for target detection. In general, target signatures should be known a priori for filter-based detection methods. However, the uncertainty of target signatures caused by the influence of atmospheric interference or other random noise degrades the detection performance. Therefore, developing a robust detection method is crucial in hyperspectral image analysis. In this study, a linearly constrained signal subspace projection approach for target detection is proposed. Instead of using a single constraint on target detection, an optimal filter with multiple constraints is designed using signal subspace projection (SSP). The SSP approach fully exploits the orthogonal property of two orthogonal subspaces; one denotes a signal subspace that contains desired targets and undesired interference, and the other denotes a noise subspace, which is orthogonal to signal subspace. By projecting the weights of the detection filter on the signal subspace, the proposed SSP reduces estimation errors in target signatures and alleviates the performance degradation caused by the uncertainty of target signatures. The SSP approach can detect desired targets, suppress undesired targets, and minimize interference effects. In this paper, three methods are provided for selecting multiple constraints of the desired target: K-means, principal eigenvectors, and endmember extraction techniques. The simulation results show that the proposed SSP with multiple constraints on the desired target selected using K-means has superior detection performance. Furthermore, the proposed SSP with multiple constraints is less sensitive to the uncertainty of target signatures.

I. INTRODUCTION

Because of advances in sensor technology, hyperspectral images containing data in hundreds of narrow spectral bands have increased in spatial and spectral resolution. In past decades, the hyperspectral image has emerged as a crucial tool used in research fields, such as mining, agriculture, and forestry (Roberts et al., 1997; Franklin, 2001; Gong and Xu, 2003; Zhan et al., 2008). Compared with multispectral images, the hyperspectral image has richer spectral information that records radiation from distinct materials. To fully exploit this characteristic, developing an efficient target detection technique that can help further analyze hyperspectral images is essential.

Hyperspectral images have been widely used in target detection applications. In these applications, targets are detected on the basis of the determination of signature numbers and target signatures in advance. Currently, numerous methods are commonly used to estimate signature numbers in distinct applications. In array signal processing, An Information-theoretic Criterion (AIC) (Akaike, 1974) and Minimum Description Length (MDL) (Rissanen, 1978; Schwarz, 1978) were proposed to identify signature numbers based on the information theory. The Harsanyi-Farrand-Chang (HFC) method, which is an eigen-thresholding method based on the Neyman-Pearson detection theory, was proposed by Harsanyi et al. (1993). The HFC method was modified (Chang and Du, 2004) to the noise-whitened HFC (NWHFC) method by using noise whitening to remove a second-order statistical correlation. Moreover, several methods are available that can be used to determine signature numbers by estimating noise covariance (Green et al., 1988; Roger, 1996; Roger and Arnold, 1996). Based on an intra-band correlation, a residual-based estimation, Residual Analysis, was proposed by Roger (1996). Conversely, based on an inter-band correlation, a Nearest-Neighbor Difference method was proposed by Green et al.

Paper submitted 02/04/14 revised 03/14/14; accepted 04/30/14. Author for correspondence: Lena Chang (e-mail: lenachang@mail.ntou.edu.tw).
[1] Department of Electrical Engineering, National Taiwan Ocean University, Keelung, Taiwan, R.O.C.
[2] Department of Communications, Navigation and Control Engineering, National Taiwan Ocean University, Keelung, Taiwan, R.O.C.

(1988). Roger and Arnold (1996) proposed a method based on a linear regression model in which the advantages of intra-band and inter-band correlations were exploited. Recently, a minimum mean square error-based method was proposed to estimate the signal subspace (Nascimento and Bioucas-Dias, 2007, 2008). In this method, named "Hyperspectral Signal identification by minimum error (HySime)," the signal and noise correlation are estimated, and the subset of eigenvalues that optimally represents the signal subspace in the least square error is selected. In the endmember extraction technique, an image is assumed to exist in an endmember, which is an ideal and pure signature of distinct classes. This technique is used to identify distinctive pixels based on two major criteria, multidimensional geometry-based and pixel spectral signature similarity. The multidimensional geometry-based methods used to determine the maximal simplex volume include N-Finder (Winter, 1999) and Simplex Growing Algorithm (SGA) (Chang et al., 2004); the methods based on the similarity of pixel spectral signature include the Automatic Target Generation Process (ATGP) (Ren and Chang, 2003), Vertex Component Analysis (VCA) (Nascimento and Bioucas-Dias, 2005), and Fully Constrained Least Squares Linear Unmixing (FCLSLU) (Heinz and Chang, 2001).

Numerous firmly established target detection algorithms have been proposed, such as Constrained Energy Minimization (CEM), Target-Constrained Interference-Minimized Filter (TCIMF), Orthogonal Subspace Projection (OSP), Noise Subspace Projection (NSP) and Signal Subspace Projection (SSP). CEM is designed as a Finite Impulse Response (FIR) filter that can be used to pass the desired target, which minimizes the output energy (Harsanyi, 1993). TCIMF was proposed (Ren and Chang, 2000) to suppress undesired targets; desired targets can be detected, undesired targets can be suppressed, and interference effects can be minimized. Furthermore, several subspace-based methods have been proposed in the last two decades. Harsanyi and Chang (1994) proposed OSP to suppress the response of background information, and the algorithm was used to match the desired target. However, the OSP design is such that information on undesired targets must be available. Compared with OSP, CEM is typically more effective in suppressing undesired targets and noise effects; however, CEM is extremely sensitive to the signature of the desired target. Furthermore, the performance of OSP and CEM are highly similar in the case of white noise with a large signal-to-noise ratio (SNR) (Du et al., 2003). Tu et al. (1998) proposed NSP based on the assumption of a weak signature of the desired target and strong interference; however, the NSP performance is degraded when the SNR is large. Chang and Yeh (1992) proposed SSP in which weights are equal to optimal weights without performing matrix inversion; SSP exhibits low sensitivity and an inaccurate signature of the desired target.

The remaining sections of this paper are organized as follows. Linearly constrained minimum variance methods are reviewed and described in Section II. A linearly constrained signal subspace projection (SSP) approach, which can alleviate the performance degradation caused by estimation errors of the desired target or other unknown interference, is proposed in Section III. Section IV presents the performance comparison of SSP and well-known target detection methods and simulations conducted using hyperspectral images. Finally, Section V draws the conclusions.

II. LINEARLY CONSTRAINED MINIMUM VARIANCE (LCMV)METHODS

Suppose that there are p desired targets and q undesired background targets. A linear spectral mixture model for a hyperspectral image pixel with L bands can be described as follows:

$$\mathbf{x} = \mathbf{S}_d \boldsymbol{\alpha}_d + \mathbf{S}_b \boldsymbol{\alpha}_b + \mathbf{n}\,, \tag{1}$$

where $\mathbf{x}$ is an L × 1 column vector, which denotes the received pixel spectral vector. In (1), $\mathbf{S}_d = [\mathbf{s}_{d_1}, \mathbf{s}_{d_2}, ..., \mathbf{s}_{d_p}]$, $\mathbf{S}_b = [\mathbf{s}_{b_1}, \mathbf{s}_{b_2}, ..., \mathbf{s}_{b_q}]$, $\boldsymbol{\alpha}_d = [\alpha_{d_1}, \alpha_{d_2}, ..., \alpha_{d_p}]^T$ and $\boldsymbol{\alpha}_b = [\alpha_{b_1}, \alpha_{b_2}, ..., \alpha_{b_q}]^T$, where '$T$' denotes the transpose operator and $\mathbf{s}_{d_i}$ and $\mathbf{s}_{b_i}$ are the ith spectral signature vectors of desired target and undesired targets with corresponding abundance fractions of α_{d_i} and α_{b_i}, respectively. In (1), $\mathbf{n}$ is interpreted as a measurement error or a model error and can be represented as additive white noise with zero mean and a covariance matrix $\sigma^2\mathbf{I}$, where $\mathbf{I}$ is an L × L identity matrix and σ^2 is the variance.

In the target detection problem, the spectral signature vector of desired targets $\mathbf{s}_{d_i}$ must be known a priori. An uncertainty of target signatures is caused by the influence of atmospheric interference or other random noise. Fig. 1(a) indicates that the same material exhibits the some variability in its spectral space representation. Fig. 1(b) presents the reflectance spectra of five randomly selected water and cane samples obtained from the MODIS/ASTER airborne simulator (MASTER) images. Fig. 1(c) shows the reflection spectra distribution in bands 10 and 25 of the water and cane. Fig. 1 demonstrates the uncertainty of a specific target signature in a hyperspectral image. In general, target detection algorithms often require an estimated desired signature, which is frequently distinct from the true signature. In practical applications, even if the true signature in a hyperspectral image is available, the matching filter-based detection algorithms may not detect all of the specific targets, particularly when the target signature is uncertain.

To detect desired targets, suppress undesired background, and minimize the interference effects simultaneously, a multiple constrained FIR linear filter was designed using the linearly constrained minimum variance (LCMV) method. The weight vector of the FIR filter is denoted by $\mathbf{w} = [w_1, w_2, \ldots, w_L]^T$, and the filter output is expressed as follows:

$$\mathbf{y} = \mathbf{w}^T \mathbf{x}\,. \tag{2}$$

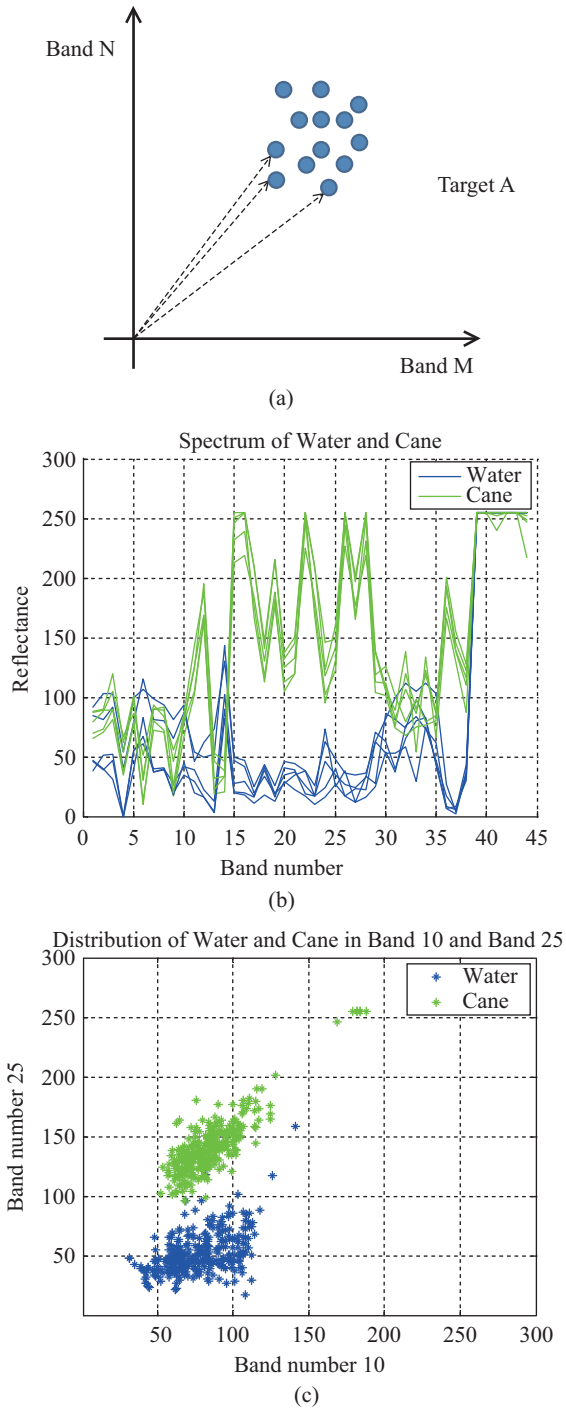

Fig. 1. Uncertainty of target signature.

The weight vector of the FIR filter was designed to minimize the filter output energy subject to the multiple linear constraints, which is defined as follows:

$$\mathbf{C}^T\mathbf{w} = \mathbf{g}\,. \tag{3}$$

In (3), $\mathbf{C} = [\mathbf{c}_1, \mathbf{c}_2, ..., \mathbf{c}_k]$ is a constraint matrix and $\mathbf{g}$ is a gain vector. The optimization problem that minimizes the filter output energy with multiple constraints shown in (3) is given as follows:

$$\min_{\mathbf{w}} \mathbf{w}^T\mathbf{R}\mathbf{w}, \quad \text{st.} \quad \mathbf{C}^T\mathbf{w} = \mathbf{g}\,, \tag{4}$$

where $\mathbf{R} = E[\mathbf{x}\mathbf{x}^T]$ is an L × L correlation matrix of the spectral vector $\mathbf{x}$. The solution of (4) obtained using LCMV is given as follows:

$$\mathbf{w}_{\mathrm{o}} = \mathbf{R}^{-1}\mathbf{C}(\mathbf{C}^T\mathbf{R}^{-1}\mathbf{C})^{-1}\mathbf{g}\,. \tag{5}$$

If a single constraint $\mathbf{d}$ is considered, the constraint matrix $\mathbf{C} = \mathbf{d}$ and gain vector $\mathbf{g} = 1$, where $\mathbf{d}$ denotes the desired target signature vector. In this case, the optimal weight is reduced to the solution of CEM:

$$\mathbf{w}_{\mathrm{CEM}} = \frac{\mathbf{R}^{-1}\mathbf{d}}{\mathbf{d}^T\mathbf{R}^{-1}\mathbf{d}}\,. \tag{6}$$

According to Du et al. (1983), CEM can detect one target at a time and is quite sensitive to the target signature $\mathbf{d}$, which is used in the constraint. To avoid the drawbacks of CEM, Ren and Chang (2000) designed a multiple constrained FIR filter, TCIMF, which chooses a constraint matrix as $\mathbf{C} = [\mathbf{D}, \mathbf{U}]$, where $\mathbf{D} = [\mathbf{d}_1, \mathbf{d}_2, ..., \mathbf{d}_p]$ and $\mathbf{U} = [\mathbf{U}_1, \mathbf{U}_2, ..., \mathbf{U}_q]$ denote the desired and undesired target signature matrices, respectively. In this case, the weight of LCMV is reduced to the solution of TCIMF:

$$\mathbf{w}_{\mathrm{TCIMF}} = \mathbf{R}^{-1}[\mathbf{D}, \mathbf{U}]([\mathbf{D}, \mathbf{U}]^T\mathbf{R}^{-1}[\mathbf{D}, \mathbf{U}])^{-1}\begin{bmatrix}\mathbf{1}_{p\times 1}\\ \mathbf{0}_{q\times 1}\end{bmatrix}. \tag{7}$$

Although TCIMF can detect desired targets and suppress undesired targets simultaneously, target signatures must be known in advance. The simulation results demonstrated that the estimation errors in the desired and undesired target signatures degraded the TCIMF performance.

III. LINEARLY CONSTRAINED SIGNAL SUBSPACE PROJECTION

LCMV-based target detection methods often require the desired target signature and undesired target signature in advance. The uncertainty of target signatures caused by the perturbation in atmospheric interference or estimation errors degrades the performance of target detection. To alleviate this performance degradation in this study, the SSP approach was proposed to design a linearly constrained FIR filter. The developed SSP method utilizes the orthogonal property of two orthogonal subspaces. One is the signal subspace which contains desired target signatures and undesired target or background interference signatures; the other is noise subspace, which is orthogonal to the signal subspace. These two sub-

spaces can be obtained through eigen-decomposition of the correlation matrix **R** of the received spectral vector **x**.

The correlation matrix **R** was eigen-decomposed as

$$\mathbf{R} = \sum \lambda_i \mathbf{e}_i \mathbf{e}_i^T = \mathbf{E}_s \mathbf{\Lambda}_s \mathbf{E}_s^T + \mathbf{E}_n \mathbf{\Lambda}_n \mathbf{E}_n^T , \quad (8)$$

where λ_i represents the eigenvalues of **R** in descending order $\lambda_1 \geq \lambda_2 \geq \ldots \lambda_{p+q} \geq \lambda_{p+q+1} = \ldots = \lambda_L = \sigma^2$ and $\mathbf{e}_i$ is the eigenvector corresponding to λ_i. In (8), $\mathbf{\Lambda}_s = \text{diag}[\lambda_1, \lambda_2, ..., \lambda_{p+q}]$, $\mathbf{\Lambda}_n = \sigma^2 \mathbf{I}_{L-p-q}$, $\mathbf{E}_s = [\mathbf{e}_1, \mathbf{e}_2, ..., \mathbf{e}_{p+q}]$, and $\mathbf{E}_n = [\mathbf{e}_{p+q+1}, \mathbf{e}_{p+q+2}, ..., \mathbf{e}_L]$. The eigenvectors corresponding to the minimum eigenvalues σ^2 are orthogonal to the target signature vectors:

$$\text{span}\{\mathbf{e}_{p+q+1}, \mathbf{e}_{p+q+2}, ..., \mathbf{e}_L\} \perp \text{span}\{\mathbf{s}_{d_1}, \mathbf{s}_{d_2} \cdots, \mathbf{s}_{d_p}, \mathbf{s}_{b_1}, \mathbf{s}_{b_2}, \cdots, \mathbf{s}_{b_q}\}. \quad (9)$$

According to the aforementioned orthogonal property, the subspace spanned by the column vectors $\mathbf{E}_n$ is denoted as the noise subspace. Its orthogonal complement span$\{\mathbf{s}_{d_1}, \mathbf{s}_{d_2}, ..., \mathbf{s}_{d_p}, \mathbf{s}_{b_1}, \mathbf{s}_{b_2}, ..., \mathbf{s}_{b_q}\}$, which is identical to the space spanned by the columns of $\mathbf{E}_s$, is referred to as the signal signature subspace.

Using the orthogonal property, the weight vector of LCMV in (5) can be rewritten as follows:

$$\mathbf{w}_o = \mathbf{R}^{-1}\mathbf{C}(\mathbf{C}^T\mathbf{R}^{-1}\mathbf{C})^{-1}\mathbf{g} = \mathbf{w}_s + \mathbf{w}_n , \quad (10)$$

where $\mathbf{w}_s = (\mathbf{E}_s\mathbf{\Lambda}_s^{-1}\mathbf{E}_s^T)\mathbf{C}[\mathbf{C}^T(\mathbf{E}_s\mathbf{\Lambda}_s^{-1}\mathbf{E}_s^T)\mathbf{C}]^{-1}\mathbf{g}$ and $\mathbf{w}_n = (\mathbf{E}_n\mathbf{\Lambda}_n^{-1}\mathbf{E}_n^T)\mathbf{C}[\mathbf{C}^T(\mathbf{E}_n\mathbf{\Lambda}_n^{-1}\mathbf{E}_n^T)\mathbf{C}]^{-1}\mathbf{g}$. In (10), $\mathbf{w}_s$ and $\mathbf{w}_n$ are the weight vector components contributed by the signal and the noise subspaces, respectively. The weight components in signal and noise subspaces can be expressed in alternative forms as follows:

$$\mathbf{w}_s = \mathbf{E}_s\mathbf{E}_s^T\mathbf{w}_o \quad (11)$$

and

$$\mathbf{w}_n = \mathbf{E}_n\mathbf{E}_n^T\mathbf{w}_o \quad (12)$$

If the constraint matrix **C** is chosen to detect the desired targets and suppress the undesired targets, exactly as the constraint matrix selected by TCIMF, **C** = [**D**, **U**]. Based on the orthogonality between the target signatures and noise subspace, the columns of the multiple constraint matrix **C** are in the signal subspace and orthogonal to $\mathbf{E}_n$:

$$\mathbf{C}^T\mathbf{E}_n = 0 . \quad (13)$$

Thus, weight vector components are contributed by the noise subspace $\mathbf{w}_n = 0$. The weight in (10) then becomes

$$\mathbf{w}_o = (\mathbf{E}_s\mathbf{\Lambda}_s^{-1}\mathbf{E}_s^T)\mathbf{C}[\mathbf{C}^T(\mathbf{E}_s\mathbf{\Lambda}_s^{-1}\mathbf{E}_s^T)\mathbf{C}]^{-1}\mathbf{g} = \mathbf{w}_s . \quad (14)$$

Eq. (14) indicates that the optimal weight of multiple constraints is equivalent to weight vector components contributed by the signal subspace. Therefore, this paper proposes the SSP approach, which uses $\mathbf{w}_s$ to design the weights of the FIR filter. The weight vector of the SSP is given as follows:

$$\mathbf{w}_{SSP} = \mathbf{E}_s\mathbf{E}_s^T\mathbf{w}_o = \mathbf{w}_s . \quad (15)$$

Practically, the ensemble correlation matrix **R** was unavailable, and the observed data were used to obtain the sample correlation matrix $\hat{\mathbf{R}}$ as follows:

$$\hat{\mathbf{R}} = \frac{1}{N}\sum_{i=1}^{N}\mathbf{x}_i\mathbf{x}_i^T , \quad (16)$$

where N is the number of samples. The sample correlation matrix was eigen-decomposed as follows:

$$\hat{\mathbf{R}} = \hat{\mathbf{E}}_s\hat{\mathbf{\Lambda}}_s\hat{\mathbf{E}}_s^T + \hat{\mathbf{E}}_n\hat{\mathbf{\Lambda}}_n\hat{\mathbf{E}}_n^T , \quad (17)$$

where $\hat{\mathbf{E}}_s$, $\hat{\mathbf{E}}_n$, $\hat{\mathbf{\Lambda}}_s$, and $\hat{\mathbf{\Lambda}}_n$ are the corresponding disturbed terms of $\mathbf{E}_s$, $\mathbf{E}_n$, $\mathbf{\Lambda}_s$ and $\mathbf{\Lambda}_n$. The weight of LCMV becomes

$$\hat{\mathbf{w}}_o = \hat{\mathbf{R}}^{-1}\mathbf{C}[\mathbf{C}^T\hat{\mathbf{R}}^{-1}\mathbf{C}]^{-1}\mathbf{g} = \hat{\mathbf{w}}_s + \hat{\mathbf{w}}_n , \quad (18)$$

where $\hat{\mathbf{w}}_s = \hat{\mathbf{E}}_s\hat{\mathbf{E}}_s^T\hat{\mathbf{w}}_o$ and $\hat{\mathbf{w}}_n = \hat{\mathbf{E}}_n\hat{\mathbf{E}}_n^T\hat{\mathbf{w}}_o$ are weight vector components in the signal and noise subspaces of $\hat{\mathbf{R}}$. The term $\hat{\mathbf{w}}_n \neq 0$ since the eigen-components of $\hat{\mathbf{R}}$ are disturbed.

Next, the SSP performance was investigated using the output signal-to-interference-plus-noise ratio (SINR), which is used to validate detection performance. The output SINR is defined as the ratio of the output energy of desired targets to the output energy of undesired targets or interference plus noise. If the desired target signature $\mathbf{s}_{d_i}$ and the undesired target signature $\mathbf{s}_{b_i}$ are also estimated from the observed samples $\mathbf{x}_i$, the noise weight vector component, $\hat{\mathbf{w}}_n$, has no influence on the filter output of desired targets and undesired targets or background interference:

$$\hat{\mathbf{w}}_n^T\mathbf{s}_{d_i} = 0 \qquad i = 1, 2, ..., p \quad (19)$$

and

$$\hat{\mathbf{w}}_n^T\mathbf{s}_{b_i} = 0 \qquad i = 1, 2, ..., q . \quad (20)$$

However, $\hat{\mathbf{w}}_n$ increases only the output noise power by $\sigma^2\hat{\mathbf{w}}_n^T\hat{\mathbf{w}}_n$. The output SINR of LCMV methods, denoted by

$\mathrm{SINR_o}$, is given as follows:

$$\mathrm{SINR_o} = \frac{\sum_{i=1}^{p} P_{d_i} \left| \hat{\mathbf{w}}_{\mathrm{o}}{}^{T} \mathbf{s}_{d_i} \right|^2}{\sum_{i=1}^{q} P_{b_i} \left| \hat{\mathbf{w}}_{\mathrm{o}}{}^{T} \mathbf{s}_{b_i} \right|^2 + \sigma^2 \hat{\mathbf{w}}_{\mathrm{o}}{}^{T} \hat{\mathbf{w}}_{\mathrm{o}}} = \frac{\sum_{i=1}^{p} P_{d_i} \left| \hat{\mathbf{w}}_{\mathrm{s}}{}^{T} \mathbf{s}_{d_i} \right|^2}{\sum_{i=1}^{q} P_{b_i} \left| \hat{\mathbf{w}}_{\mathrm{s}}{}^{T} \mathbf{s}_{b_i} \right|^2 + \sigma^2 (\hat{\mathbf{w}}_{\mathrm{s}}{}^{T} \hat{\mathbf{w}}_{\mathrm{s}} + \hat{\mathbf{w}}_{\mathrm{n}}{}^{T} \hat{\mathbf{w}}_{\mathrm{n}})}, \quad (21)$$

where $P_{d_i} = E[\boldsymbol{\alpha}_{d_i}{}^2]$ and $P_{b_i} = E[\boldsymbol{\alpha}_{b_i}{}^2]$. The output SINR of SSP, denoted by $\mathrm{SINR_{SSP}}$, is given as follows:

$$\mathrm{SINR_{SSP}} = \frac{\sum_{i=1}^{p} P_{d_i} \left| \hat{\mathbf{w}}_{\mathrm{s}}{}^{T} \mathbf{s}_{d_i} \right|^2}{\sum_{i=1}^{q} P_{b_i} \left| \hat{\mathbf{w}}_{\mathrm{s}}{}^{T} \mathbf{s}_{b_i} \right|^2 + \sigma^2 \hat{\mathbf{w}}_{\mathrm{s}}{}^{T} \hat{\mathbf{w}}_{\mathrm{s}}}. \quad (22)$$

By comparing (21) with (22),

$$\mathrm{SINR_{SSP}} > \mathrm{SINR_o}. \quad (23)$$

The result in (23) shows that the proposed SSP approach has a large output SINR than LCMV-based methods. Moreover, this large output SINR increases the probability of target detection.

The effect of finite samples on the SSP was then analyzed. If one desired target is constrained, the output SINR of LCMV is given as follows (Chang and Yeh, 1992):

$$\mathrm{SINR_o} = \frac{P_d}{P_{bo} + P_{no} + \frac{L-1}{N} P_d}, \quad (24)$$

where P_{d} denotes the output power of the desired target and P_{bo} and P_{no} denote the output power of background signature and noise power, respectively, calculated by the optimal weight $\mathbf{w}_{\mathrm{o}}$. The output SINR of SSP is given by

$$\mathrm{SINR_{SSP}} = \frac{P_d}{P_{bo} + P_{no} + \frac{p+q-1}{N} P_d}. \quad (25)$$

When the output SINR reaches one-half of the SINR of the optimal filter, the sample sizes required for LCMV and SSP are given as follows:

$$N \geq L^2 \mathrm{SNR_{input}} \quad (26)$$

Table 1. Projection values between $\mathbf{s}_d$ and $\mathbf{s}_i$.

Signature name	Projection values (a)	Projection values (b)
Pinon_Pine ANP92-14A ndl	1 (desired signature)	0.7838
Clinochlore_Fe SC-CCa-1.b	0.4393	0.8629
Lizardite NMNHR4687.d < 30	0.7974	0.9828
Nontronite NG-1.a	0.7838	1 (desired signature)
Goethite WS219 (limonite)	0.6515	0.9670

and

$$N \geq (p+q-1) L \mathrm{SNR_{input}}, \quad (27)$$

where $\mathrm{SNR_{input}}$ is the input SNR. In general, $p + q < L$, and (26) and (27) indicate that SSP has an improved convergence rate compared with that of LCMV-based methods.

IV. EXPERIMENTAL RESULTS AND DISCUSSIONS

In this section, experiments are presented to validate the performance of the proposed SSP. The performance of the proposed SSP is compared with that of CEM, TCIMF, and OSP by using three types of hyperspectral data set: United States Geological Survey (USGS) digital spectral library (Clark et al., 2003), MASTER, and ROSIS image data. In Experiment 1, hyperspectral data with 224 spectral bands from the USGS digital spectral library were used to examine the convergence rate and output SINR of the proposed method. In Experiment 2, the effect of various multiple constraints on the SSP performance was investigated using the test image data, which were obtained from a plantation area in Auku on the west coast of Taiwan by using the MASTER airborne simulator in 2000. In Experiment 3, the detection performance was examined using the test image data which was acquired from University of Pavia in Italy by using the ROSIS instrument in 2001. In the simulations, two SSP scenarios were considered. One with a single unit gain constraint on the desired target signature denoted as SSP-SC, and the other with multiple constraints, including unit gain, on the desired target signature and null gain on undesired targets denoted as SSP-MC.

Experiment 1

In this experiment, the convergence rate and filter output SINR of the proposed approach were compared with those of other subspace-based methods by using hyperspectral data from the USGS digital spectral library. We selected five signatures, one desired target $\mathbf{s}_d$, and four undesired targets or background interference $\mathbf{s}_i$, i = 1, 2, ..., 4 (Table 1).

The reflectance of the five signatures are shown in Fig. 2. In the simulations, noise is an additive white noise, the SNR of the desired signature is 20 dB, and the interference-to-noise

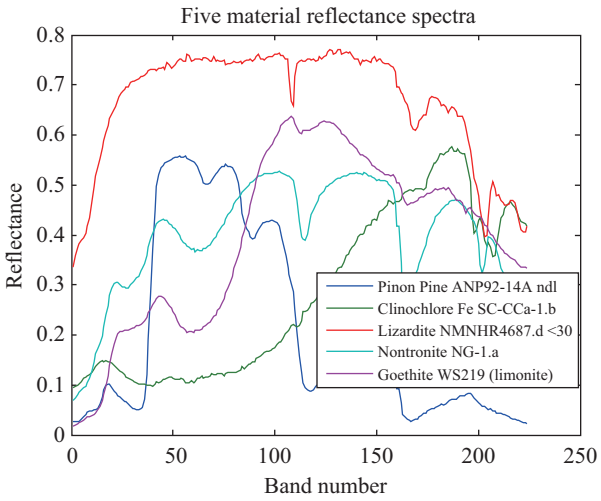

Fig. 2. Reflectance spectra of the five signatures.

ratio (INR) of the interference signatures is 10 dB. To examine the effect of background interference on the SSP performance, we used a projection value between $\mathbf{s}_d$ and $\mathbf{s}_i$ to indicate the separation between the desired and interference signatures. Two simulation scenarios were considered. One with a large projection value indicates that the desired and interference signature vectors are close to each other, and the other, with a small projection value, indicates that the desired and interference signature vectors are distinct. The projection values between $\mathbf{s}_d$ and $\mathbf{s}_i$ are presented in Table 1. In these simulations, a unit gain constraint on the desired target signature $\mathbf{s}_d$ was applied to CEM and SSP-SC; four undesired targets, $\mathbf{s}_i$, i = 1, 2, ..., 4, were considered to form a desired orthogonal subspace projector for OSP; and a multiple constraint matrix $\mathbf{C} = [\mathbf{s}_d, \mathbf{s}_1, \mathbf{s}_2, \mathbf{s}_3, \mathbf{s}_4]$ and a gain vector $\mathbf{g} = [1, 0, 0, 0, 0]^T$ are used in the TCIMF and SSP-MC methods.

First, we conducted simulations with exactly known target signatures. Fig. 3 shows the averaged output SINR from 300 Monte Carlo trials for various samples. According to Fig. 3, the output SINRs of OSP were almost constant for various samples because OSP is performed using known interference signatures. For a single constraint, the proposed SSP-SC possessed larger output SINRs and improved convergence rates than CEM. Similarly, for multiple constraints, SSP-MC had higher output SINRs and faster convergence rates than TCIMF. This simulation result is consistent with the theoretic analysis of (23). According to Fig. 3(a), the sample size required for SSP-MC and TCIMF in convergence approached 1000 and 3500, respectively, which is also consistent with the analysis result of (27). Comparing Fig. 3(a) with Fig. 3(b), all output SINRs decreased for the simulation scenario with a large projection value. However, performance of SSP-MC and SSP-SC remains superior to that of TCIMF and CEM. Moreover, the performance of SSP-MC approached that of OSP in convergence. The simulation results in Fig. 3 indicate that SSP-MC has a considerable improvement in output SINR,

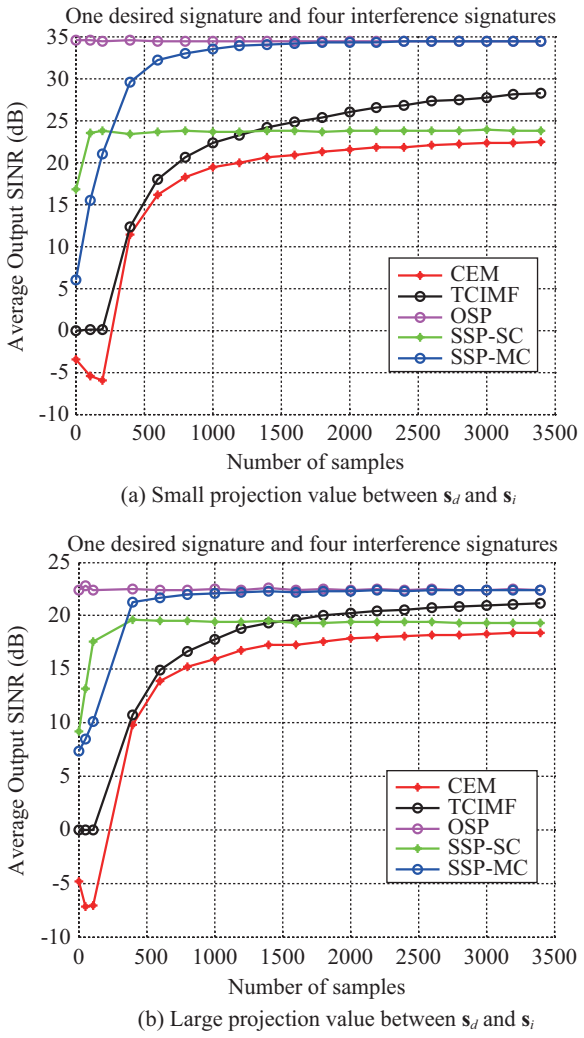

Fig. 3. Average output SINR versus number of samples; exact $\mathbf{s}_d$ and exact $\mathbf{s}_i$.

particularly for small sample size. We then performed simulations with a known desired signature and interference signatures estimated by the ATGP endmember extraction algorithm. Fig. 4 presents the averaged output SINR versus number of samples. Comparing the results in Fig. 4 with those in Fig. 3, the output SINRs of OSP and TCIMF decreased the most considerably. These results imply that OSP and TCIMF are more sensitive to the estimated interference signatures. In addition, CEM and SSP-SC have similar output SINRs (Figs. 3 and 4) because CEM and SSP-SC require only unit gain constraint on the desired target.

Experiment 2

In this experiment, the effect of selecting multiple constraints on the SSP performance was investigated using one MASTER image with 44 spectral bands. The test image data acquired from an area in Auku on the west coast of Taiwan (Fig. 5(a)) was chosen for the simulations. The ground truth data of five land cover types are displayed in Fig. 5(b).

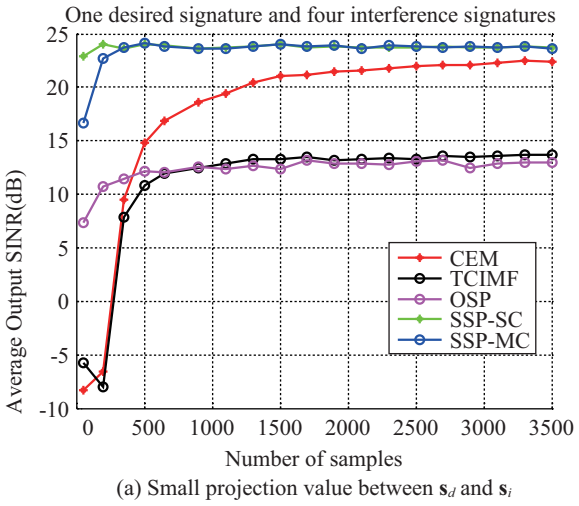

(a) Small projection value between $\mathbf{s}_d$ and $\mathbf{s}_i$

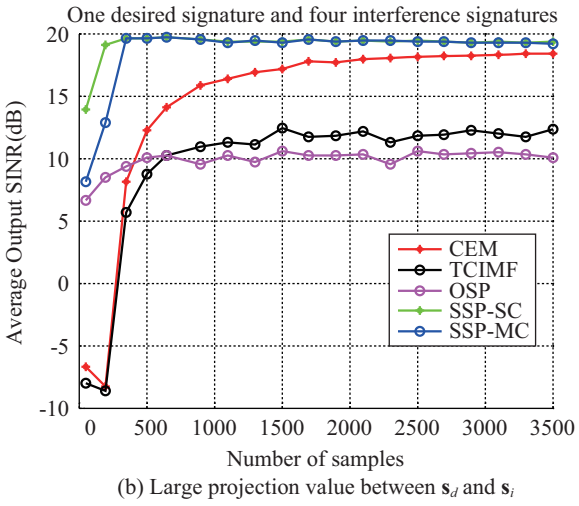

(b) Large projection value between $\mathbf{s}_d$ and $\mathbf{s}_i$

Fig. 4. Average output SINR versus number of samples; exact $\mathbf{s}_d$ and estimated $\mathbf{s}_i$.

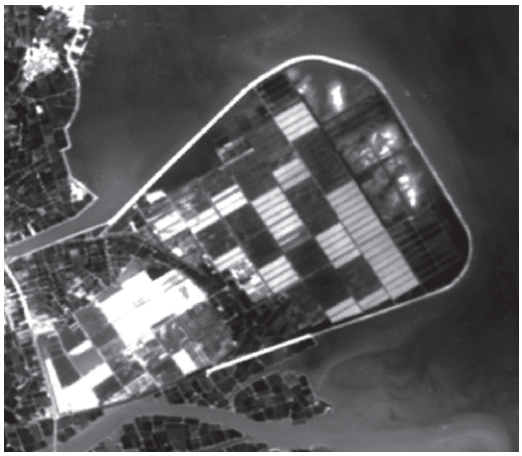

(a) Test image, Auku

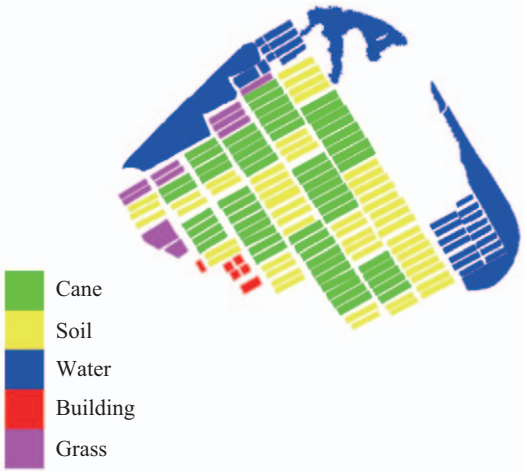

(b) Ground truth data

Fig. 5. Test image.

According to the description of Fig. 1 and the simulation results of Fig. 4, the uncertainty of target signatures degraded the performance of filter-based detection methods. To alleviate this performance degradation, we proposed the use of multiple constraints, which may cover the spectral variations of a material. In the following sections, three methods of multiple constraint selection are presented for a material.

(1) Multiple constraints selected using K-means (MCK): First, the observed data for one material were spatially segmented into regions by using the K-means algorithm. Segmentation was performed until the variance of each region was less than the threshold. The mean vector in each region was then extracted as one constraint of the desired target. Because the observed data belonged to the same material, the target signatures were extremely close. A threshold value of 0.002 was selected as the variance threshold for the K-means algorithm in the simulations.

(2) Multiple constraints selected using principal eigenvectors (MCE): Based on the correlation matrix of the observed data, principal eigenvectors were selected by eigen-decomposing the correlation matrix. The principal component vectors were selected to preserve 99.5% energy and were treated as multiple constraints of the desired target.

(3) Multiple constraints selected using endmembers (MCM): Based on pixel spectral signature similarity, the endmember extraction technique was used to identify endmembers, which were treated as multiple constraints of the desired target. In the simulations, the ATGP algorithm was used to extract the endmembers.

Next, the performance of multiple constraints selected by MCK, MCE, and MCM were examined using MASTER test data, including materials cane, soil, water, building, and grass shown in the Auku image. The detection results are presented in Figs. 6-10. In addition, the performance of CEM, which uses mean vector as a single constraint, was examined. Table 2 presents the detection precision. Experimental results are as follows.

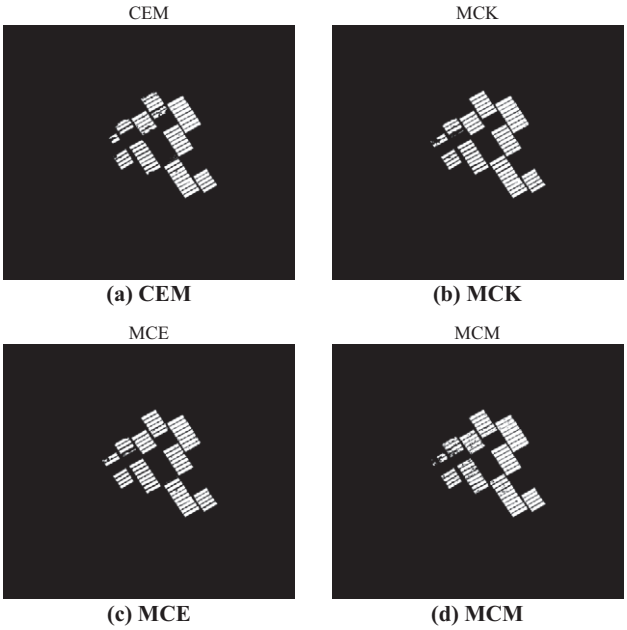

(a) CEM (b) MCK

(c) MCE (d) MCM

Fig. 6. Detection results of cane.

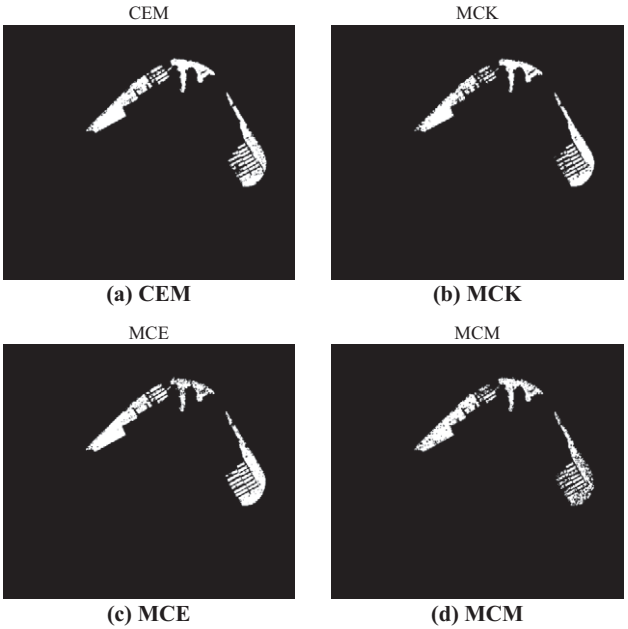

(a) CEM (b) MCK

(c) MCE (d) MCM

Fig. 8. Detection results of water.

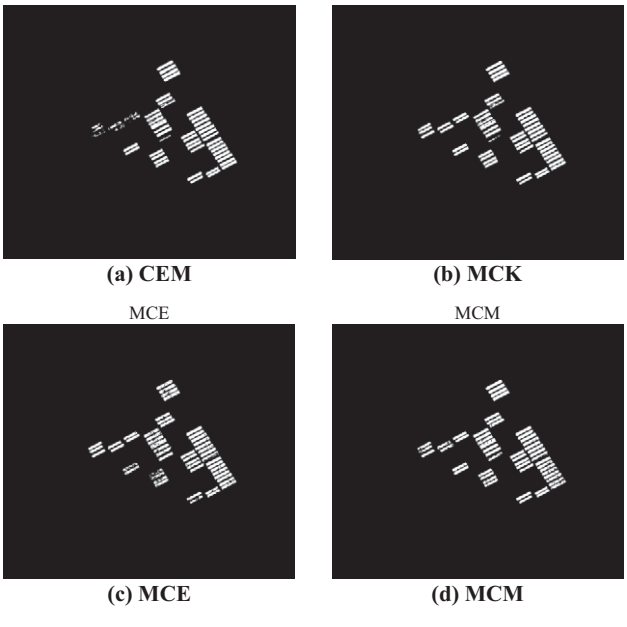

(a) CEM (b) MCK

(c) MCE (d) MCM

Fig. 7. Detection results of soil.

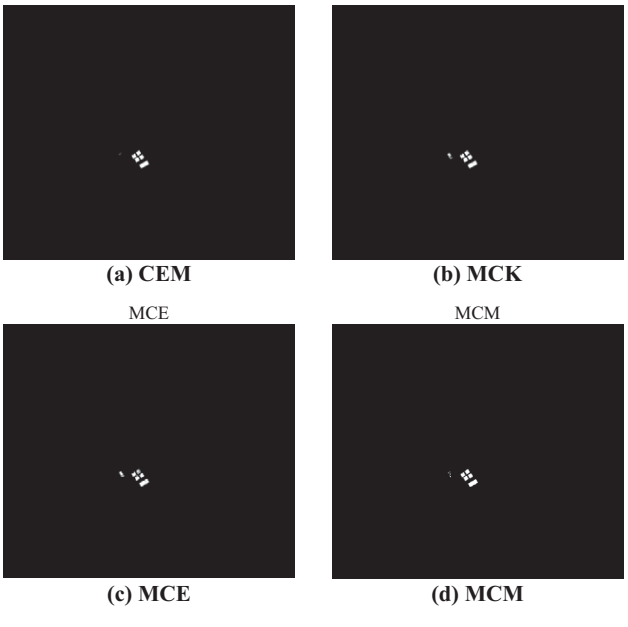

(a) CEM (b) MCK

(c) MCE (d) MCM

Fig. 9. Detection results of building.

(1) On average, the performance of MCK was superior to MCE and MCM because MCK considers spectral and spatial information concurrently. Furthermore, the mean vector constraints selected by MCK can cover the observed data of the desired target even if they possess a large variation.
(2) For high uncertainty in the target signature, a small amount of the observed data with a large variation could not be included in the principal components. This induces the performance degradation of MCE.
(3) The MCM performance was the worst because it involved pixel-based detection. The sensitivity of this approach to the uncertainty of the desired target signature was the same as that of CEM.
(4) Target detection based on multiple constraints on the desired target was superior to that based on a single constraint on the desired target. The results show that the selection of multiple constraints affected the detection performance.

The performance of target detection was then evaluated

Table 2. Detection precision of CEM, MCK, MCE and MCM.

	CEM	MCK	MCE	MCM
Cane	90.27%	91.28%	90.22%	83.58%
Soil	88.41%	94.75%	90.65%	91.33%
Water	85.01%	83.93%	84.87%	78.56%
Building	86.88%	94.23%	90.03%	90.29%
Grass	83.49%	90.63%	85.02%	88.50%
Average	86.81%	90.96%	88.16%	86.45%

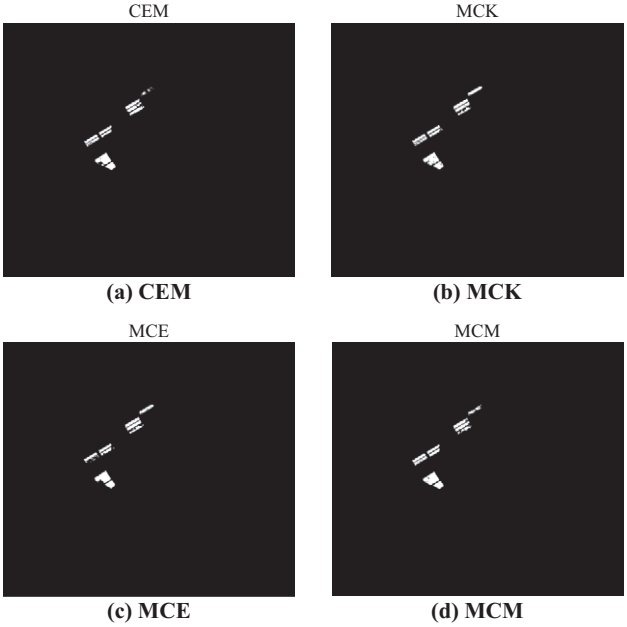

(a) CEM (b) MCK (c) MCE (d) MCM

Fig. 10. Detection results of grass.

using MASTER images. In simulations, we examined detection precision with 5% constant false alarm. The target signatures were estimated using two simulation sample sizes; 1) a small sample size with 150 randomly selected testing samples from each data type, and 2) a large sample size with 500 randomly selected testing samples from each data type. The sample mean signature from each data type was treated as the desired signature. In CEM, TCIMF, OSP, and SSP-SC, one sample mean signature was selected as the desired target signature. The remaining mean signatures were treated as undesired target signatures. SSP-MC uses multiple constraints on the desired target, which includes a sample mean signature and other constraints extracted using the MCK. Table 3 presents the detection precision averaged from 300 Monte Carlo trials.

Tables 3(a) and 3(b) show the detection probability with a 5% constant probability of false alarm (PFA) for small and large sample sizes, respectively. Comparing the results in Tables 3(a) and 3(b), the performance of CEM and TCIMF was degraded significantly for the small sample size. This degradation is attributable to the deviation of a sample correlation matrix. As the sample size increases, the detection

Table 3. Detection precision of CEM, TCIMF, OSP, SSP-SC, and SSP-MC.

	CEM	TCIMF	OSP	SSP-SC	SSP-MC
Cane	87.13%	87.91%	80.96%	91.87%	93.84%
Soil	94.08%	91.92%	90.51%	94.48%	95.03%
Water	94.37%	95.72%	93.36%	96.15%	96.84%
Building	88.52%	89.27%	83.22%	89.54%	92.78%
Grass	75.85%	76.20%	72.01%	76.74%	80.20%

(a) testing sample number = 150, PFA = 5%

	CEM	TCIMF	OSP	SSP-SC	SSP-MC
Cane	91.33%	93.87%	82.29%	92.53%	94.00%
Soil	94.9%	93.07%	90.49%	95.47%	96.53%
Water	99.13%	99.20%	96.61%	99.27%	99.30%
Building	93.60%	93.60%	87.84%	92.07%	98.07%
Grass	83.27%	82.27%	74.81%	83.20%	85.43%

(b) testing sample number = 500, PFA = 5%

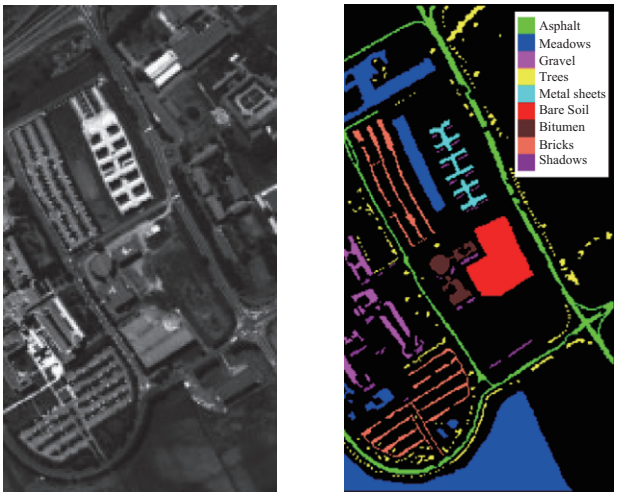

(a) Test image of the University of Pavia (b) Ground truth

Fig. 11. Test image.

precision is improved sequentially. Because of the estimation error in the undesired target signatures, the OSP performance was the worst for the small sample size. The situation slightly improved for OSP (Table 3(b)). The results in Table 3 indicate that SSP-MC outperformed SSP-SC for five land cover types in both simulation sample sizes. This conclusion reveals that multiple desired target constraints demonstrate stronger performance than a single desired target constraint for minimizing the uncertainty of a target signature.

Experiment 3

In this experiment, the second real hyperspectral image data that were acquired by the ROSIS instrument in 2001 were used to examine the performance of target detection. Fig. 11(a) shows the test image of the University of Pavia, Italy. The

Table 4. Detection precision of CEM, TCIMF, OSP, SSP-SC and SSP-MC.

	CEM	TCIMF	OSP	SSP-SC	SSP-MC
Asphalt	84.80%	83.64%	81.92%	91.09%	92.17%
Meadows	81.60%	88.00%	82.40%	83.40%	88.60%
Gravel	79.57%	83.84%	80.11%	87.37%	87.60%
Trees	91.74%	91.83%	91.51%	92.09%	91.89%
Painted metal sheets	99.20%	99.89%	99.39%	99.93%	99.93%
Bare Soil	87.95%	90.12%	81.15%	89.15%	91.40%
Bitumen	83.10%	84.80%	81.74%	88.40%	89.20%
Self-Blocking Bricks	91.80%	91.00%	89.55%	92.10%	93.00%
Shadows	90.55%	93.15%	89.65%	91.45%	93.20%

image size is 610 × 340, and it has 103 spectral bands; 12 bands were removed because of noise and water absorption. The ground truth of the test image is displayed in Fig. 11(b). Nine cover-type data, asphalt, meadows, gravel, trees, painted metal sheets, bare soil, bitumen, self-blocking bricks, and shadows, were included in the experiment. The selection of desired and undesired signatures is the same as that in Experiment 2. Considering sufficient samples in the simulation, 500 testing samples were randomly selected for each cover type. The detection probability with 5% constant PFA is presented in Table 4 in which the detection precision is averaged from 300 Monte Carlo trials.

The results shown in Table 4 are consistent with those in Tables 2 and 3. The proposed SSP method has a higher detection probability than the others. The results reveal that the estimation errors in target signatures can be reduced using the SSP approach. Furthermore, SSP-MC consistently outperformed SSP-SC, thus implying that the SSP-MC with multiple constraints on the desired target is more robust for minimizing the uncertainty effect of target signatures in real image data.

V. CONCLUSION

In this study, we proposed a linearly constrained SSP approach for target detection by using hyperspectral images. We designed an optimal FIR filter with multiple constraints by using the SSP approach. This approach alleviates the performance degradation caused by the estimation errors of the desired target or unknown interference. The convergence rate and output SINR of the proposed SSP were analyzed in this study. Simulations indicated that the proposed SSP approach has a faster convergence rate and larger output SINR than the widely established target detection methods, CEM, TCIMF, and OSP, when hyperspectral data from the USGS digital spectral library are used.

To alleviate the performance degradation in target detection caused by the uncertainty of desired target signatures, multiple constraints were used on the desired target. Simulations validated by real image data indicated that a more satisfactory performance is achieved using multiple target constraints selected by MCK, and the proposed SSP method has a higher detection probability than other methods. SSP reduces estimation errors in target signature and increases the detection precision. Furthermore, SSP-MC with multiple target constraints selected by MCK is a robust detection approach, which can overcome the uncertainty of desired target signatures in real image data.

REFERENCES

Akaike, H. (1974). A new look at the statistical model identification. IEEE Transactions Automatic Control 19, 716-723.

Chang, C. I. and Q. Du (2004). Estimation of number of spectrally distinct signal sources in hyperspectral imagery. IEEE Transactions on Geoscience and Remote Sensing 42, 608-619.

Chang, C. I., C. C. Wu, W. M. Liu and Y. C. Ouyang (2006). A new growing method for simplex-based endmember extraction algorithm. IEEE Transactions on Geoscience and Remote Sensing 44, 2804-2819.

Chang, L. and C. C. Yeh (1992). Performance of DMI and eigenspace-based beamformers. IEEE Transactions on Antennas and Propagation 40, 1336-1347.

Clark, R. N., G. A. Swayze, R. Wise, K. E. Livo, T. M. Hoefen, R. F. Kokaly and S. J. Sutley (2003). USGS Digital Spectral Library splib05a, USGS Open File Report 03-395.

Du, Q., H. Ren and C. I. Chang (2003). A comparative study for orthogonal subspace projection and constrained energy minimization. IEEE Transactions on Geoscience and Remote Sensing 41, 1525-1529.

Franklin, S. E. (2001). Remote Sensing for Sustainable Forest Management. Lewis Publishers and CRC Press, Florida.

Gong, P. and Xu, B. (2003). Remote sensing of forests over time, Kluwer Academic Publishers, 301-334.

Green, A. A., M. Berman, P. Switzer and M. D. Craig (1988). A transformation for ordering multispectral data in terms of image quality with implications for noise removal. IEEE Transactions on Geoscience and Remote Sensing 26, 65-74.

Harsanyi, J. C. (1993). Detection and classification of subpixel spectral signatures in hyperspectral image sequences, Ph.D. Thesis, Department of Electrical Engineering, Maryland Baltimore County University, Baltimore, MD.

Harsanyi, J. C. and C. I. Chang (1994). Hyperspectral image classification and dimensionality reduction: an orthogonal subspace projection approach. IEEE Transactions on Geoscience and Remote Sensing 32, 779-785.

Harsanyi, J. C., W. Farrand and C. I. Chang (1993). Determining the number and identity of spectral endmembers: An integrated approach using Neyman-Pearson eigenthresholding and iterative constrained RMS error minimization. Proceeding of the 9th Thematic Conference Geologic Remote Sensing, Michigan, US, 395-408.

Heinz, D. and C. I. Chang (2001). Fully constrained least squares linear mixture analysis for material quantification in hyperspectral imagery. IEEE Transactions on Geoscience and Remote Sensing 39, 529-545.

Nascimento, J. and J. Bioucas-Dias (2005). Vertex component analysis: a fast algorithm to unmix hyperspectral data. IEEE Transactions on Geoscience and Remote Sensing 43, 898-910.

Nascimento, J. and J. Bioucas-Dias (2007). Hyperspectral signal subspace estimation. IEEE International Geoscience and Remote Sensing Symposium, Barcelona, Spain, 3225-3228.

Nascimento, J. and J. Bioucas-Dias (2008). Hyperspectral subspace identification. IEEE Transactions on Geoscience and Remote Sensing 46, 2435-2445.

Ren, H. and C. I. Chang (2000). A target-constrained interference-minimized approach to subpixel detection for hyperspectral images. Optical Engineering 39, 3138-3145.

Ren, H. and C. I. Chang (2003). Automatic spectral target recognition in hyperspectral imagery. IEEE Transactions on Aerospace and Electronic

Systems 39, 1232-1249.

Rissanen, J. (1978). Modeling by shortest data description. Automatica 14, 465-471.

Roberts, D. A., R. O. Green and J. B. Adams (1997). Temporal and spatial patterns in vegetation and atmospheric properties from AVIRIS. Remote Sensing of Environment 62, 223-240.

Roger, R. E. (1996). Principal components transform with simple, automatic noise adjustment. International Journal of Remote Sensing 17, 2719-2727.

Roger, R. E. and J. F. Arnold (1996). Reliability estimating the noise in AVIRIS hyperspectral images. International Journal of Remote Sensing 17, 1951-1962.

Schwarz, G. (1978). Estimating the dimension of a model. Annals of Statistics 6, 461-464.

Tu, T. M., C. H. Chen and C. I. Chang (1998). A noise subspace projection approach to target signature detection and extraction in an unknown background for hyperspectral images. IEEE Transactions on Geoscience and Remote Sensing 36, 171-181.

Winter, M. E. (1999). N-FINDR: an algorithm for fast autonomous spectral end-member determination in hyperspectral data. Proceeding of SPIE 3753, Imaging Spectrometry V, Denver, United States of America, 266-275.

Zhan, Y. J., G. D. Hu and Y. Y. Wu (2008). Hyperspectral remote sensing rock and mineral spectral feature mining based on rough set theory. IEEE proceeding of Computer Science and Software Engineering 4, 470-473.